This is a repository copy of *Early stages of fat crystallisation evaluated by low-field NMR and small-angle X-ray scattering*.

Ladd Parada Marjorie (Orcid ID: 0000-0003-1355-649X)

Rondeau-Mouro Corinne (Orcid ID: 0000-0002-8573-1050)

Early stages of fat crystallisation evaluated by low field NMR and Small-Angle X-ray Scattering

Marjorie Ladd Parada[a]*, Megan J. Povey[a], Josélio Vieira[b], Michael Rappolt[a], and Michael E. Ries[c]

[a] School of Food Science and Nutrition, University of Leeds, LS2 9 JT, Leeds, U.K.

[b] Nestlé, Product Technology Centre, YO31 8FY, York, U.K.

[c] School of Physics and Astronomy, University of Leeds, LS2 9JT, Leeds, U.K.

*Corresponding author: Marjorie Ladd Parada, School of Food Science and Nutrition, University of Leeds, LS2 9 JT, Leeds, U.K., e-mail: marladdp@gmail.com

Abstract

Low field time-domain NMR (20 MHz) is commonly used in the studies of fats in the form of solid fat content (SFC) measurements. However, it has the disadvantage of low sensitivity to small amounts of crystalline material (0.5%), thus often incorrectly determining crystallisation induction times. From spin-lattice relaxation rate measurements (R_1) during the isothermal crystallisation measurements of cocoa butter between 0.01 and 10 MHz using fast field cycling NMR we learnt previously, that the most sensitive frequency region is below 1 MHz. Thus, we focused on analysing our 10 kHz data in detail, by observing the time-dependence of R_1 and comparing it to standard SFC_{NMR} and SFC determinations from Small Angle X-ray Scattering (SFC_{SAXS}). Although not reflecting directly the SFC, the R_1, at this low frequency is very sensitive to changes in molecular aggregation, and hence potentially serving as an alternative for determination of crystallisation induction times. Alongside R_1, we also show that SFC_{SAXS} is more sensitive to early stages of crystallisation, that is, standard SFC_{NMR} determinations become more relevant when crystal growth starts to dominate the crystallisation process but fail to pick up earlier crystallisation steps. This paper thus demonstrates the potential of studying triacylglycerols at frequencies below 1 MHz for obtaining further understanding of the early crystallisation stages of fats, and presents an alternative and complementary method to estimate SFC by SAXS.

1. Introduction

Vegetable fats are a key ingredient in a variety of industries, especially in confectionary. Of these fats, cocoa butter (CB) is particularly of interest as it is one of the main components in chocolate, and when crystallised in the right form, provides chocolate with its main sensory and stability characteristics[1]; thus, the interest in studying its crystallisation process from structural and kinetic perspectives. For the former, X-ray scattering remains the most unambiguous technique for identification of the six different crystal polymorphs (γ, α, β'-III, β'-IV, β-V and β-VI in order of increasing stability) of CB [2-4]. Therefore, it is frequently used to understand the structural evolution of CB, though the intensity of the Bragg peaks has occasionally been used to track crystallisation development [5-7].

For fat crystallisation kinetics, time domain (TD) NMR techniques at 20 MHz are commonly used for the determination of solid fat content (SFC). In fact, it has become a standard in the American Oil Chemist's Society -AOCS- (USA) methods, applying either the direct or the indirect method [8]. The direct method is usually preferred over the indirect method because of its robustness, i.e. it is not sensitive to sample temperature or weight, unlike the indirect method. Briefly, the direct method is based on the principle that after 70 μs only the liquid signal (S_L) is obtained, as the solid signal (S_S) decays quickly. Therefore, it is possible to obtain the SFC from the ratio of the solid component intensity divided by the total NMR intensity. Given that there is an inherent dead time, the signal is corrected by a factor (f) as shown in equation 1:

$$SFC_{NMR} = \frac{f(S_{S+L} - S_L)}{f(S_{S+L} - S_L) + S_L} \cdot 100\% \tag{1}$$

where (S_{S+L}) is the (measured) combined signal of the solid and the liquid components. In contrast, the indirect method measures only the liquid signal of the sample and compares it to the signal of a fully molten sample [9-12].

However, whilst widely accepted, TD-NMR has the disadvantage of not being sensitive at low SFC values (<0.5%)[11, 13, 14] thus reducing its applicability for studying nucleation and determining induction times. These are usually better determined by other methods such as scanning diffusive light scattering and polarised light microscopy[13], though differential scanning calorimetry (DSC) and TD-NMR methods remain the staple for kinetic studies, not only in industry, but also in most fat crystallisation publications [15-19]. Regardless of the lower sensitivity of the SFC_{NMR} method for small SFC values, this technique is particularly popular,

since it only requires a low-resolution bench-top NMR equipment. However, we will demonstrate that relaxation measurements at lower frequencies can provide additional information on the molecular organisation of the system.

The main components of fats, triacylglycerols (TAGs), can be considered to be branched polymers, so it is plausible to hypothesise that their dynamics cover orders of magnitude in time, and thus frequencies, similarly to other polymers, and even phospholipids [20-23]. Moreover, Eads *et al.*[24] reported that structural differences in TAGs are observable at frequencies between tens to hundreds of kHz. Namely, using quadrupole echo deuterium NMR spectra recorded at 61.4 MHz, they observed that spin-lattice relaxation time (T_1) is sensitive to the molecular motions of the methyl groups of the different polymorphs, being less restricted in the less stable crystal polymorphs. Therefore, it is of interest to study TAGs at a range of relatively low frequencies.

Considering that for practical and economic reasons, there is a large interest in developing bench-top techniques for food analysis [25-27], it is important to not only focus on different frequencies, but also in those attainable with bench-top equipment. In our previous paper[28], we explored the application of fast field cycling NMR (FFC-NMR) for the determination of the diffusion coefficients of CB at different temperatures. However, we also performed isothermal experiments on CB initially molten to 50 °C and cooled to 22 °C, as a first evaluation of the feasibility of using spin lattice relaxation rate (R_1) measurements at very low frequencies (< 10 MHz) to track the early stages of molecular organisation in triacylglycerols. The results were promising, as the R_1 values in the region below 1 MHz increased as time progressed [28]. Therefore, in this paper we have analysed the R_1 trends in further detail and compared their behaviour to the SFC evolutions (i) as determined routinely by NMR (SFC$_{NMR}$) and (ii) as shown in this work, by small angle X-ray scattering (SFC$_{SAXS}$).

2. Materials and Methods

As in our previous paper[28], refined, bleached and deodorised West-African CB (Cocoa de Zaan, The Netherlands) was used in all experiments without any further refinement.

2.1. Fast-Field Cycling NMR

In our previous paper[28], we performed isothermal measurements at 22 °C of CB initially heated to 50 °C and cooled in a step-wise manner to allow for temperature equilibration and

full relaxation. We chose this set of data rather than that of the 100 °C treatment because of the larger variation of R_1 observed.

The reader is referred to our previous publication for further experimental details[28]. Briefly, ^{1}H NMR dispersion (NMRD) profiles were obtained using a Stelar SMARtracer FFC NMR Relaxometer (Stelar s.r.l., Mede, PV, Italy). Measurements were undertaken approximately every 6 min at 22 °C for two hours. Polarisation and acquisition fields of 7 MHz were used, with a polarisation time and recycle delay of $5T_1$. Field switching time was 2.5 ms, while the spectrometer dead time was 15-20 μs. The relaxation field was in the range of 0.01-10.0 MHz. Non-prepolarised sequences were applied between 10.0 and 1.6 MHz, whilst prepolarised sequences were applied between 1.6 and 0.01 MHz.

It was evident in our previous paper, that the NMRD profiles changed as the isothermal time progressed. The first measurement at 22 °C resembles those at the higher temperatures, suggesting that it is representative of self-diffusion (SD). Therefore, we hypothesise that the NMRD profiles are descriptive of SD and provide additional insight on relaxation mechanism at lower frequencies. We have considered that this mechanism might be that of order director fluctuations (ODF) or layer undulations (LU) as commonly observed in liquid crystals[29, 30] and lipid bilayers[31], having dependencies of $R_1 \propto 1/\sqrt{\nu}$ and $R_1 \propto 1/\nu$, respectively.

Therefore, as a first step towards in-depth studies of the NMRD profiles, the data at 8 min and 2 h of isothermal time was fitted with equation 2.

$$(R_1)_{TOTAL} = (R_1)_{SD} + (R_1)_{ODF \ or \ LU} \tag{2}$$

where $(R_1)_{SD}$ is calculated from[32]

$$\left(R_1(\nu)\right)_{SD} \cong R_1(0) - B\sqrt{\nu} = R_1(0) - N\left(\frac{\mu_0}{4\pi}\gamma_H^2\hbar\right)^2 \left(\frac{\sqrt{2}+8}{30}\right)\left(\frac{\pi}{D}\right)^{\frac{3}{2}}\sqrt{\nu} \tag{3}$$

where ν is the frequency, N the number of nuclei per cubic metre (in this case hydrogen), μ_0 is the permeability of free space, γ_H is the gyromagnetic factor of hydrogen, $\hbar$ is the reduced Planck's constant, and D is the self-diffusion coefficient. As the self-diffusion coefficient would not be expected to increase over time due to increasing solidification, B was constrained to $B \geq 5.02$ which was the fitted value for the 8 min NMRD profile. N was taken from Ladd-Parada, *et al* (2018).[28]

The ODF can be described by

$$\left(R_1(v)\right)_{ODF} = \frac{A_{ODF}}{\sqrt{v}}\left[f\left(\frac{v_{ODFmax}}{v}\right) - f\left(\frac{v_{ODFmin}}{v}\right)\right] \tag{4}$$

where A_{ODF} is the prefactor depending on temperature; the order parameter; inter-proton distances; and viscoelastic properties of the material. v_{ODFmax} and v_{ODFmin} are the high and low frequency limits and f*(y)* is the cut -off function[29]:

$$f(y) = \frac{1}{\pi}\left[arctan(\sqrt{2y} + 1) + arctan(\sqrt{2y} - 1) - arctan\left(\frac{\sqrt{2y}}{y+1}\right)\right] \tag{5}$$

The LU are defined by equation 6, which uses the same frequency limits as the ODFs, since they are a restricted version of the latter. Thus, LU were only considered for fitting the NMRD profiles, as their occurrence is less likely at the beginning of the crystallisation process.

$$\left(R_1(v)\right)_{LU} = \frac{A_{LU}}{v\pi}\left[arctan\left(\frac{v_{ODFmax}}{v}\right) - arctan\left(\frac{v_{ODFmin}}{v}\right)\right] \tag{6}$$

2.2. Solid Fat Content from TD-NMR

Solid fat content (SFC) measurements were performed in a Minispec-mq$_{one}$ SFC analyser (Bruker BioSpin, GmbH, Rheinstetten, Germany), at 20 MHz, using the direct method AOCS Cd 16b-93[8].

Glass NMR tubes were filled with ca. 1.5 mL of CB. Samples were held at 50 °C for 15 minutes, and cooled down step-wise to 22 °C, allowing for 15 min for temperature equilibration. Once 22 °C were reached, measurements were performed every 5 minutes for two hours.

2.3. X-ray Scattering Set-Up and SFC from SAXS

A disposable quartz capillary of 1.5 mm in diameter was filled with molten CB (50 °C), and left at ambient temperature for a week, prior to measurements. The samples were treated using the same thermal protocol as that for the NMR measurements.

Small and wide-angle X-ray scattering (SAXS and WAXS) measurements were performed in a SAXSpace instrument (Anton Paar GmbH, Graz, Austria) equipped with a Cu-anode that operates at 40 kV and 50 mA ($\lambda = 0.154$ nm). The scattering vector *q* was calibrated with silver-behenate. A sample-detector distance of 317 mm was used, allowing the measurement of scattering vectors of 0.1-18 nm^{-1}. The 1D scattering patterns were recorded with a Mythen

micro-strip X-ray detector (Dectris Ltd, Baden, Switzerland). All measurements were made with an exposure time of 7 minutes for a total amount of two hours.

Polymorphs were identified based on the peak positions in the small and wide-angle regions and compared to values in literature[2, 3, 6], and the amount of crystallised material was estimated from the small angle region as follows:

The amount of material in the fluid state is proportional to the diffuse scattering contribution centred at $q = 2.55$ nm^{-1} in the SAXS regime[33]. Thus, to determine the fraction of material in the molten state, we determined the intensity (area under the curve), I_{liquid}, of this scattering contribution from 1.8 to 3.2 nm^{-1} for all scattering patterns (see Figure 1), and normalised this data by setting the first I_{liquid} to unity. We note that I_{liquid} drops from initially 1.00 to a final value of 0.65.

For the solid phase, the first order Bragg peaks were then likewise area-integrated to obtain the corresponding intensities, I_{solid} (Figure 1) of the solid material. Since all the material is assumed to be either solid or molten ($I_{liquid} + I_{solid} = 1$), we set the final $I_{solid} = 0.35$ (Figure 1), and normalised all other I_{solid} values by this final value. Finally, for determining the SFC, we applied the following equation:

$$SFC_{SAXS} = \frac{I_{solid}}{I_{solid} + I_{liquid}} \cdot 100\% \hspace{2cm} (7)$$

The resulting fractions of crystalline material where then plotted vs time and analysed for crystallisation kinetics as described in the next section.
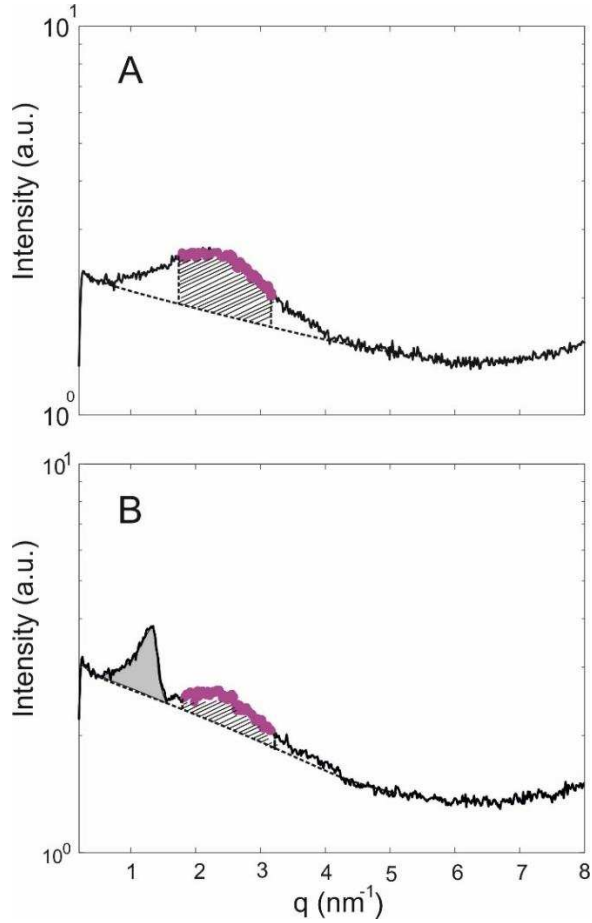
Figure 1. SAXS pattern displaying the molten state of cocoa butter (A) and the partially solidified sample after 2 hours of isothermal equilibration at 22 °C (B). Diffuse scattering arising from the molten phase is highlighted with solid pink circles, and its intensity is identified by the area shown with hatched lines. In panel B, the area integrated for the first order Bragg peak is shown in grey. A dashed line has been included in both panels, representing the applied baselines.

2.4. Crystallisation kinetics analysis

Different crystallisation kinetics models are available. The Avrami model is the most frequently used, describing the changes in volume of crystals as a function of time, as

$$F = \frac{V - V_0}{V_m - V_0} = 1 - e^{-Bt^k} \qquad (8)$$

where V is the volume of the crystals, V_0 is the initial crystal volume, V_m is the maximum crystal volume at the end of the crystallisation process, B is the Avrami constant (dependent on nucleation of new particle and growth rate) and k is the Avrami exponent dependent on the

dimensionality of particle growths. Note, *k* can take values between 1 and 4, e.g. k = 3 for two-dimensional plate-like crystal growth.

Compared to the Avrami ansatz, Gompertz or Foubert's models fit the data with a significantly improved goodness (reduced chi-squared tested)[34, 35]. In addition, in our study, a full plateau was not reached within the two hours of analysis. This made it impossible to get a good fit as in the Avrami's equation the final crystallised proportion is a set parameter, thus introducing further error.

The failure to achieve a plateau value is not a problem when applying the Gompertz equation (equation 4) as the maximum proportion of crystalline material attained (*m*), here referred as SFC, is one of the fitted parameters, rather than a pre-established one, enabling a better fit. Therefore, these fits are the ones we report here, but we refer the reader to the Supplementary Information for the fits using the Avrami equation (table S1) [35].

$$f(t) = m \cdot exp\left(-exp\left(\frac{\mu e}{m}(\lambda - t) + 1\right)\right) \qquad (9)$$

where *f(t)* is the amount of crystalline material at time, *t*, *m* is the amount of crystalline material as *t* approaches infinity, μ is the maximum increase rate in crystallisation (the tangent to the inflection point of the crystallisation curve), λ is a measure for the induction time (intercept of the tangent at the inflection point with the time-axis) and *e* is the Euler's number 2.7183.

The two methods used for describing the crystallisation kinetics (Eq. 3 and 4) were applied for SFC_{NMR} and SFC_{SAXS} measurements (Figure 2 and Figure S1). Fits were performed using a least squares approach, using Matlab R2017A® (MathWorks Inc., Massachusetts, USA) with 95% confidence levels.

3. Results

From the X-ray scattering data, we firstly identified the developing polymorphs, from both SAXS and WAXS, as shown in Figure 2.
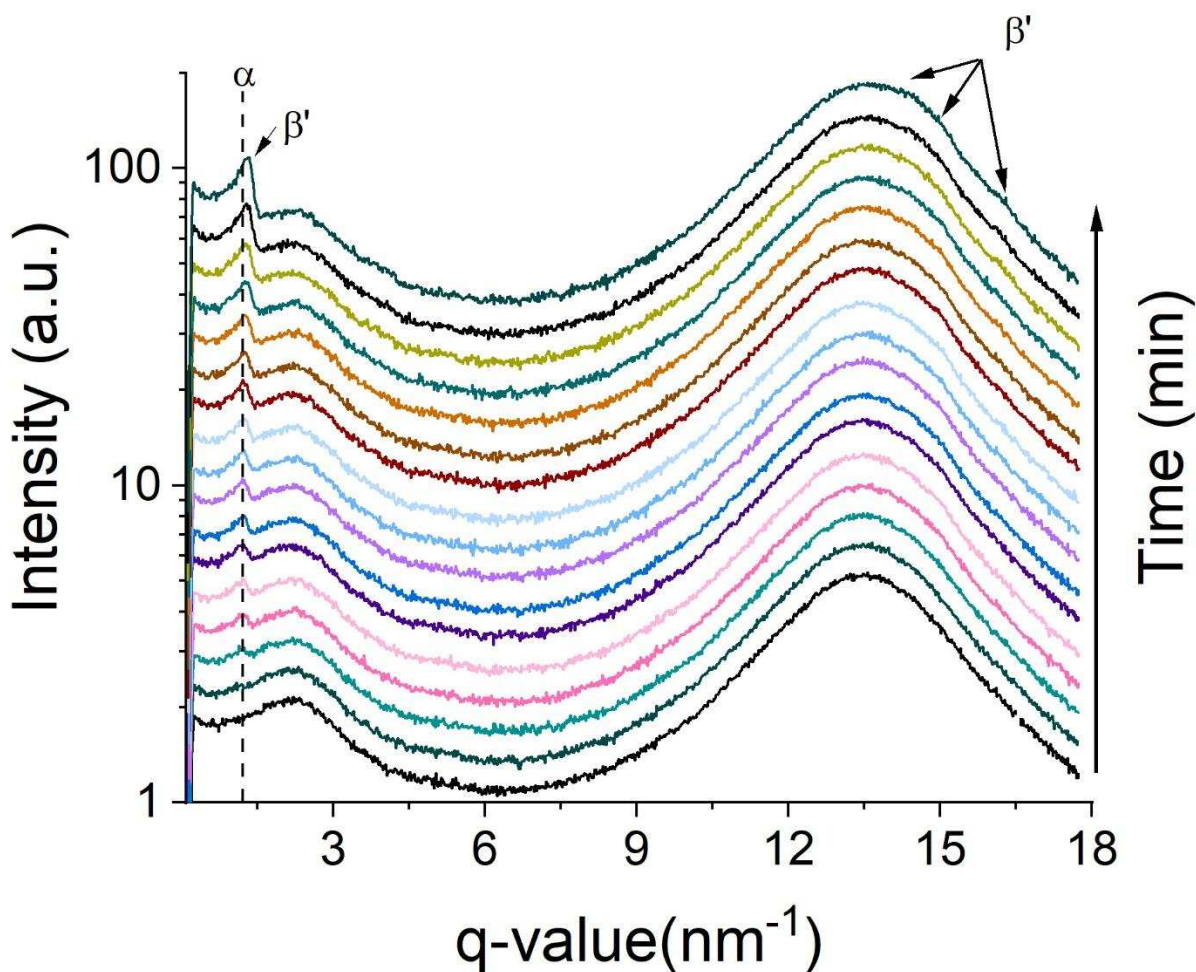
Figure 2 Small and wide-angle X-ray Scattering of CB held isothermally at 22 °C. Every pattern represents a 7 minute measurement. The dashed line indicates the position of the first order diffraction peak of the α-polymorph, the arrow in the SAXS region is indicating the peak position of the β'-polymorph. The arrows in the WAXS region are displaying the positions where the β'-polymorph peaks are usually observed and where broad peaks are present.

After 14 minutes, a first SAXS diffraction peak is observed arising from the α-phase formation (q = 1.25 nm^{-1}), identified by the dashed line in Figure 2. Then, after 35 min this peak shifts to a q value of 1.35 nm^{-1} indicating the presence of the β'-polymorph. The corresponding d-spacing of the α- and β'-polymorphs are 5.03 nm and 4.65 nm, respectively. Thus, both displaying a 2L-stacking (L refers to one fatty acid monolayer) with chains being non-tilted in the α-phase and tilted in the β'-phase (the tilt angle is given by $\cos^{-1}(4.65/5.03) = 22°$). In the wide-angle region, a small broad peak developed after 28 minutes, between 14.2 and 15.3 nm^{-1}, i.e. covering the region related to that of α-polymorph peak (15.14 nm^{-1}). After approximately 70 minutes, another broad peak developed between 15.8 and 16.8 nm^{-1} suggesting small traces of the β'-polymorph formation. These traces are more evident when superimposing the final and first scattering patterns (see Supplementary Information, Figure S2).

The SFC$_{NMR}$ measurements (Figure 3A) showed a single crystallisation event, in the form of a sigmoidal curve, which only started reaching a plateau at an SFC value of 45% after 120 min. The estimated induction time of this event is an hour (Table 1). This is to some extent in contrast to what is observed in the SFC$_{SAXS}$ (Figure 3B). In agreement with literature[4, 6, 7, 36], the latter displays two crystallisation events, the first one reaching a plateau at about 8% after 40 min, and the second one still displaying an exponential growth, starting at approximately an hour, similarly to the SFC data, reaching a fraction of 0.35, but without plateauing even after 2 h. This solid fraction is smaller than the SFC measured by NMR, but still in good agreement with previous reports[7, 37].

From the FFC NMR measurements, the R_1 values at frequencies between 0.01 and 10 MHz were plotted versus time (see Supplementary Information, Figure S3), confirming that frequencies below 1 MHz are the most sensitive to structural changes in CB. We note that the R_1 values at 10 MHz seem to display a slight decreasing trend, however, this is still within experimental error (Figure 3C, squares). Contrastingly, the relaxation rates at 10 kHz (Figure 3C, circles) showed the largest sensitivity, increasing almost in a four-fold manner.
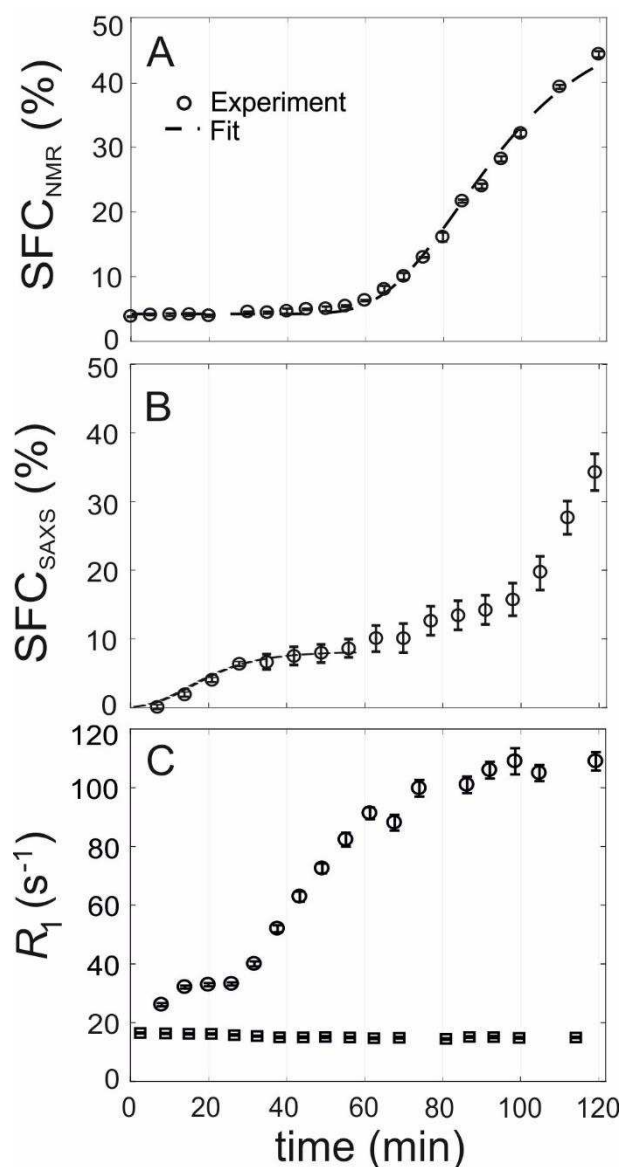
Figure 3. Crystallisation of CB at 22 °C. (A) SFC_{NMR} turnover and the corresponding Gompertz fit. (B) SFC_{SAXS} plot and the Gompertz fit of the first crystallisation event, which has not been captured by SFC_{NMR}. (C) R_1 values at 10 kHz (circles) and 10 MHz (squares).

Interestingly, during the first 30 minutes an increase of R_1 is observed that displays a first plateau from 20 to 30 min. Whilst more points are needed to fully confirm the increase of R_1 from zero to 20 s^{-1}, the plateau at 35 s^{-1} is confirmed by three data points. This is in agreement with a two-step process, as observed by SAXS (Fig. 3B). However, the lack of sufficient data points for $t < 10$ min, does not allow to determine the starting point (induction time) accurately. Still, we can consider that the increase of R_1 starts prior to the first measurement, and that it stabilises after approximately 20 min. This is followed by the second region, which starts to plateau at 110 s^{-1} after approximately one hour (Figure 1 C). In summary, it seems to follow the same trend as the SFC_{SAXS} curve, but with an earlier onset, and particularly, a faster change

rate during the second crystallisation event. We note, however, that we do not suggest that R_1 is directly proportional to SFC, but that it is sensitive to changes occurring within our samples, as will be discussed in the following section in more detail.

Table 1. Gompertz fits of the main turnover step (deduced from SFC_{NMR}) and the first crystallisation event (deduced from SFC_{SAXS}).

Regarding the estimated parameters, the induction times (λ) differ between the two events, with the first at $\lambda = 9$ min and the second at $\lambda = 64$ min, respectively. In terms of the conversion rate, the main turnover is about two times faster.

From the analysis of the NMRD profiles, it is possible to observe that at 8 min (Figure 4A), the main observable relaxation mechanism is that of SD, as would be expected. Both the total (continuous line) and SD (dash-dotted line) overlap almost completely, suggesting that there might be a small contribution from another type of molecular motion, possibly the ODFs. After 2h of holding CB isothermally at 22 °C (Figure 4 B and C), it becomes clear that SD is no longer the only relaxation mechanism at play. From the fit of equations 2-6, it is easily seen that the ODF function fits the experimental data better than the LU (Figure 4C), suggesting that the former is more likely to be the origin of the observed changes, as expected from the initial linear fits (see Supplementary Information Figure S4). Additionally, the fitted v_{ODFmax} (Table 2) corresponds approximately to the region that is better described by the ODF than the SD (Figure 4B).
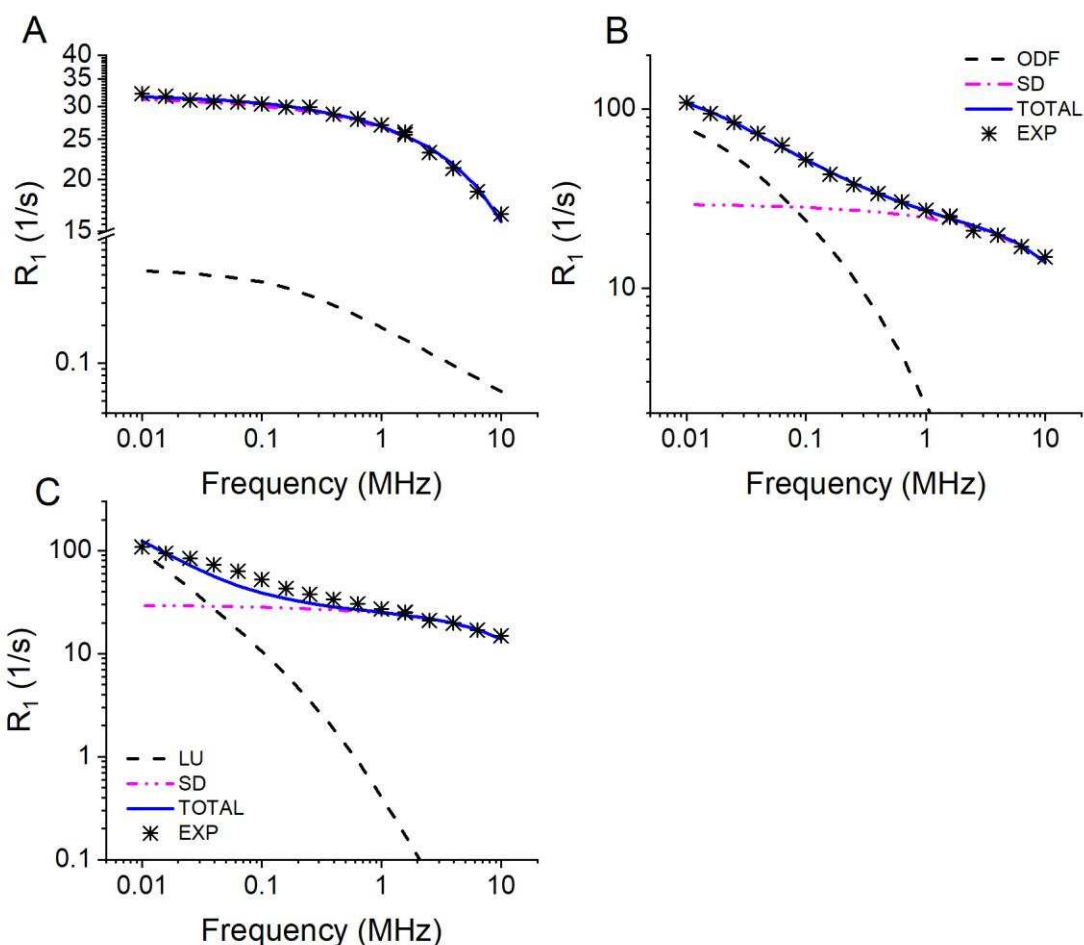
Figure 4 NMRD curves of CB held isothermally at 22 °C for 8 min (panel A) and 2 h (panels B and C). Panels A and B show the experimental (stars) curves fitted (continuous line) with equation 2, the dash-dotted line represents the self-diffusion component, and the dashed line the ODF component. In panel C, the data was fitted similarly, but instead of the ODF collective motions, the data was fitted with a combination of SD (dash-dotted line) and layer undulation functions (dashed line).

Table 2 Fitted parameters obtained from the best fits of Equation 2 to the experimental R_1 NMRD profiles of cooled CB held isothermally at 22 °C for either 8 min or 2 h.

4. Discussion

In agreement with literature, SFC_{NMR} was the least sensitive technique to the initial stages of crystallisation in CB (Figure 1A), and only displayed one crystallisation event in contrast to the other two techniques (SFC_{SAXS} and R_1 at 10kHz). That is, the SFC_{NMR} method is a robust method to measure the final solid fat content and displays well the later stages of crystal growth, but early crystallisation events might be obscured. Indeed, the role of solidification by the α-phase formation is overlooked in this method.

From the SFC_{SAXS} (Figure 1B), the α-phase turnover (starting at 14 min) and, later, the concomitant formation of the β'-phase are both depicted. However, the maximum crystalline fraction was estimated to be 35% compared to 45% from SFC_{NMR}. Even if these values can be considered satisfactorily close, in future studies we will try to identify possible reasons for this mismatch between the obtained SFC values. As an additional note, we draw attention to the SAXS peaks developing prior to the WAXS peaks (Figure 3), indicating that lamellar arrangement occurs prior to the packing of the fatty acid chains, as has been observed by previous workers [5, 38].

Interestingly, the R_1 at 10 kHz behaves qualitatively similarly to the SFC_{SAXS} (Figure 1C and B), but the onset and plateau of the two events occur at an earlier stage. We suggest that the changes in slope in the R_1 curve precede the SFC_{SAXS} plot events because it is not directly dependent on the proportion of solid material, but rather to the amount of TAGs undergoing orientational ordering and their associated dynamics, which includes a great part of the non-solid material. Therefore, once the sample has transformed into a crystalline network with a general orientation, no large changes are observable at 10 kHz, but are at 20 MHz, which seems to be sensitive to crystal growth.

In our previous paper [28], the application of FFC-NMR allowed us to investigate CB over a wide range of very low ^{1}H NMR frequencies (< 10 MHz). Under the conditions used, we observed that frequencies between 0.01 and 1 MHz were the most sensitive for detecting the early stages of the phase change. From the range of frequencies available, we selected 10 kHz, as it showed the largest increase in R_1 values over time (Figure 3C), thus indicating that this frequency is most sensitive to the early stages of crystallisation. The overall increasing trend with time of R_1 (that is, the decrease of T_1) at all frequencies is well understood, since it reflects the process of solidification leading to an increased viscosity because of the higher amount of solids, and the continuous decrease of mobility of the molecules as they transition from fully synclinical to periplanar conformations. Therefore, molecular tumbling slows down and with it, the correlation time increases. We note, Adam-Berret et al. (2009)[39] also observed an initial increase of R_1, but at later stages of the crystallisation a decrease in R_1 was recorded. They argue that this is due to a reduction in relaxation sinks, which hinders spin diffusion in the later stages of crystallisation. This second stage of crystallisation, was not seen in our experiments, because the SFC was only followed up to 50%, i.e., a large amount of fluid TAGs remained and also we did not capture in our experiments the perfecting of the crystals[39, 40].

More specifically, from our NMRD analysis (Figure 4) we consider that the increase of R_1 at very low frequencies is related to order director fluctuations [21, 41, 42], similarly to what has been observed previously in nematic and smectic phases [22, 43, 44]. These order director fluctuations could be explained in the light of our newly proposed model of the structured clusters of molten TAGs[33] [37]. Briefly, TAGs are thought to assemble in clusters immersed in an isotropic medium of TAGs from which some molecules start interacting with the outer fatty acids, thus creating an additional layer, or shell, which increases in coverage as temperature decreases. These clusters might begin to orientate once a crystallisation-inducing temperature (such as 22 °C) is reached, generating some of the first lamellar structures. Presently, we have only compared ODFs and LU, but other relaxation mechanisms might come into play, such as individual motions deriving from defects within the fatty acid chains, as proposed for phospholipid bilayers [22, 45, 46], especially during the later stages of crystallisation which will require further studies.

5. Conclusions and further work

In this work, we have confirmed that tracking the R_1-values at 10 kHz allows us to observe the initial stages of crystallisation as it is sensitive to the amount of orientationally ordered TAG molecules and their associated dynamics in the sample. Hence, the alignment of molten TAG clusters, should lead to a significant increase in R_1. Therefore, for future validation studies, it is not necessary to study the full range of frequencies available to FFC-NMR equipment but rather selecting 20 MHz for standard SFCs and 10 kHz for probing early changes of molecular motions allowing to record highly time-resolved and complementary data sets. When the whole crystallisation process is the subject of interest, i.e. including crystal growth, SFC and T_1 measurements at 20 MHz are advisable as they are more sensitive to the later stages of crystallisation. Noteworthy, both the R_1 method of this study and the newly introduced SFC$_{SAXS}$ determination display both the two-step transition involving the early formation of the α-phase followed by the formation of the β'-polymorph.

Finally, to increase the breadth of information on molecular motions obtained from low frequency measurements, it would be of interest to perform second magnetic moment calculations, as previously reported by Berret, *et al.* [47]. T_1 measurements at frequencies between 10 and 20 MHz, and above this frequency are also relevant for obtaining information of all the different molecular motions that are involved in the crystallisation process. T_2 measurements could also usefully be performed, as spin-spin relaxation has been related[48] to

changes in the surface area of the crystalline material over time (at a constant SFC) and thus are relevant to the evaluation of the sensitivity of this parameter during the initial phases of crystallisation.

6. Acknowledgements

7. References

[1] S.T. Beckett, Chocolate Manufacture, in: G. Talbot (Ed.), Science and Technology of Enrobed and Filled Chocolate, Confectionery and Bakery Products, Woodhead Publishing**2009**, pp. 11-28.

[2] R.L. Wille, E.S. Lutton, *Journal of the American Oil Chemists Society* **1966** *43*(8) 491-496.

[3] G.M. Chapman, E.E. Akehurst, W.B. Wright, *Journal of the American Oil Chemists Society* **1971** *48*(12) 824-830.

[4] K. van Malssen, R. Peschar, H. Schenk, *Journal of the American Oil Chemists' Society* **1996** *73*(10) 1209-1215.

[5] C. Loisel, G. Keller, G. Lecq, C. Bourgaux, M. Ollivon, *Journal of the American Oil Chemists' Society* **1998** *75*(4) 425-439.

[6] K. van Malssen, A. van Langevelde, R. Peschar, H. Schenk, *Journal of the American Oil Chemists' Society* **1999** *76*(6) 669-676.

[7] K. Dewettinck, I. Foubert, M. Basiura, B. Goderis, *Crystal Growth & Design* **2004** *4*(6) 1295-1302.

[8] AOCS,Official methods and recommended practices of the AOCS, AOCS, Champaign, Ill, 1998.

[9] K.P.A.M.v. Putte, J.v.d. Enden, *Journal of Physics E: Scientific Instruments* **1973** *6*(9) 910.

[10] K. Van Putte, J. Van Den Enden, *Journal of the American Oil Chemists Society* **1974** *51*(7) 316-320.

[11] S. Martini, M.L. Herrera, A. Marangoni, *Journal of the American Oil Chemists Society* **2005** *82*(5) 313-317.

[12] B. BioSpin, Solid Fat Content (SFC) Analysis, 2014. https://www.bruker.com/fileadmin/user_upload/8-PDF-Docs/MagneticResonance/TD-NMR/SFC_AppNote_T151922.pdf. 2017).

[13] M. Cerdeira, R.J. Candal, M.L. Herrera, *Journal of Food Science* **2004** *69*(9) R185-R191.

[14] D.J. McClements, M.J.W. Povey, *International Journal of Food Science & Technology* **1988** *23*(2) 159-170.

[15] I.T. Norton, C.D. Lee-Tuffnell, S. Ablett, S.M. Bociek, *Journal of the American Oil Chemists' Society* **1985** *62*(8) 1237-1244.

[16] C. Simoneau, M.J. McCarthy, D.S. Reid, J.B. German, *Trends in Food Science & Technology* **1992** *3* 208-211.

[17] K. Sato, *Chemical Engineering Science* **2001** *56*(7) 2255-2265.

[18] W. MacNaughtan, I.A. Farhat, C. Himawan, V.M. Starov, A.G.F. Stapley, *JAOCS, Journal of the American Oil Chemists' Society* **2006** *83*(1) 1-9.

[19] C. Himawan, W. MacNaughtan, I.A. Farhat, A.G.F. Stapley, *European Journal of Lipid Science and Technology* **2007** *109*(1) 49-60.

[20] R.A. Pethrick, T. Amornsakchai, A.M. North, Introduction to Molecular Motion in Polymers, in: N.o.m.m.i. polymers (Ed.), Introduction to Molecular Motion in Polymers, Whittles Publishing**2011**, pp. 19-37.

[21] F. Noack, *Progress in Nuclear Magnetic Resonance Spectroscopy* **1986** *18*(3) 171-276.

[22] R. Kimmich, E. Anoardo, *Progress in Nuclear Magnetic Resonance Spectroscopy* **2004** *44*(3–4) 257-320.

[23] M. Flämig, M. Hofmann, A. Lichtinger, E.A. Rössler, *Magnetic Resonance in Chemistry* **2019** *0*(0).

[24] T.M. Eads, A.E. Blaurock, R.G. Bryant, D.J. Roy, W.R. Croasmun, *Journal of the American Oil Chemists' Society* **1992** *69*(11) 1057-1068.

[25] B.P. Hills, Applications of Low-Field NMR to Food Science, in: G.A. Webb (Ed.), Annual Reports on NMR Spectroscopy, Academic Press**2006**, pp. 177-230.

[26] E. Kirtil, S. Cikrikci, M.J. McCarthy, M.H. Oztop, *Current Opinion in Food Science* **2017** *17* 9-15.

[27] F. Capozzi, M.A. Cremonini, C. Luchinat, G. Placucci, C. Vignali, *Journal of Magnetic Resonance* **1999** *138*(2) 277-280.

[28] M. Ladd-Parada, M.J. Povey, J. Vieira, M.E. Ries, *Molecular Physics* **2018** 1-8.

[29] E. Carignani, L. Calucci, E. Juszyńska-Gałązka, M. Gałązka, M. Massalska-Arodź, C. Forte, M. Geppi, *The Journal of Physical Chemistry B* **2016** *120*(22) 5083-5092.

[30] P.J. Sebastião, A. Gradišek, L.F.V. Pinto, T. Apih, M.H. Godinho, M. Vilfan, *The Journal of Physical Chemistry B* **2011** *115*(49) 14348-14358.

[31] C.C. Fraenza, C.J. Meledandri, E. Anoardo, D.F. Brougham, *ChemPhysChem* **2014** *15*(3) 425-435.

[32] D. Kruk, R. Meier, E.A. Rössler, *Physical Review E* **2012** *85*(2) 020201.

[33] A. Sadeghpour, M.L. Parada, J. Vieira, M. Povey, M. Rappolt, *The Journal of Physical Chemistry B* **2018** *122*(45) 10320-10329.

[34] I. Foubert, P.A. Vanrolleghem, B. Vanhoutte, K. Dewettinck, *Food Research International* **2002** *35*(10) 945-956.

[35] I. Foubert, K. Dewettinck, P.A. Vanrolleghem, *Trends in Food Science & Technology* **2003** *14*(3) 79-92.

[36] A. Rigolle, B. Goderis, K. Van Den Abeele, I. Foubert, *Journal of Agricultural and Food Chemistry* **2016** *64*(17) 3405-3416.

[37] M. Ladd Parada, A. Sadeghpour, J. Vieira, M. Povey, M. Rappolt, *The Journal of Physical Chemistry B* **2018** *122*(45) 10330-10336.

[38] S. Ueno, A. Minato, H. Seto, Y. Amemiya, K. Sato, *The Journal of Physical Chemistry B* **1997** *101*(35) 6847-6854.

[39] M. Adam-Berret, A. Riaublanc, C. Rondeau-Mouro, F. Mariette, *Crystal Growth & Design* **2009** *9*(10) 4273-4280.

[40] J.W. Lubach, D. Xu, B.E. Segmuller, E.J. Munson, *Journal of Pharmaceutical Sciences* **2007** *96*(4) 777-787.

[41] R.Y. Dong, *The Journal of Physical Chemistry* **1996** *100*(39) 15663-15669.

[42] K.H. Schweikert, F. Noack, *Molecular Crystals and Liquid Crystals Science and Technology. Section A. Molecular Crystals and Liquid Crystals* **1992** *212*(1) 33-44.

[43] S.R. M., K. Jean- Pierre, F. Gianni, B. Salvatore, *Magnetic Resonance in Chemistry* **2016** *54*(6) 502-509.

[44] R. Kimmich, N. Fatkullin, *Progress in Nuclear Magnetic Resonance Spectroscopy* **2017** *101* 18-50.

[45] R. Kimmich, A. Peters, *Journal of Magnetic Resonance (1969)* **1975** *19*(2) 144-165.

[46] R. Kimmich, G. Voigt,Defect Diffusion Models in NMR and Dielectric Relaxation, Zeitschrift für Naturforschung A, 1978, p. 1294.

[47] M. Adam-Berret, C. Rondeau-Mouro, A. Riaublanc, F. Mariette, *Magnetic Resonance in Chemistry* **2008** *46*(6) 550-557.

[48] M. Adam-Berret, M. Boulard, A. Riaublanc, F. Mariette, *J Agric Food Chem* **2011** *59*.

Table 1. Gompertz fits of the main turnover step (deduced from SFC_{NMR}) and the first crystallisation event (deduced from SFC_{SAXS}).

Parameter	SFC_{SAXS}	SFC_{NMR}
λ	8.8 ± 3.4 (min)	63.9 ± 0.02 (min)
m	8.3 ± 0.8 (%)	56.60 ± 0.09 (%)
μ	0.33 ± 0.10 (min^{-1})	0.78 ± 0.04 (min^{-1})

Table 2. Fitted parameters obtained from the best fits of Equation 2 to the experimental R_1 NMRD profiles of cooled CB held isothermally at 22 °C for either 8 min or 2 h.

Fitted Parameter	8 min	2h
B (a.u.)	5.02 ± 0.2	5.01 ± 0.2
D (10^{-12} m^{2}s^{-1})	5.59 ± 0.2	5.59 ± 0.2
A_{ODF} (s^{-2})	0.099773	11.54 ± 0.6
A_{LU} (s^{-2})	---	2.40 ± 0.3
$\upsilon_{ODFmax}(10^3\,MHz)$	2.39 ± 0.39	0.59 ± 0.04
$\upsilon_{ODFmin}(10^{-2}\,MHz)$	0.09 ± 0.04	0.30 ± 0.04

8. TOC Graphic Abstract